Quartz Pendulous Accelerometers for Navigation and Tactical Grade Systems

J. Beitia, A. Clifford, C. Fell, P. Loisel

InnaLabs® Ltd
Blanchardstown Industrial Park, Snugborough Rd
Blanchardstown, Dublin 15
IRELAND

Inertial Sensors and Systems 2015
Karlsruhe, Germany

978-1-4673-6738-7/15/$31.00 © 2015

Abstract

Accelerometers which are integrated into navigation, guidance or piloting systems are required to meet very demanding performance requirements in terms of accuracy, stability and linearity. Typically these requirements must be achieved under stringent conditions, at sea, on land, in air, and over the full life cycle of the system. Therefore not surprisingly, only two technologies so far have risen to the challenge and have demonstrated the right capabilities: Vibrating Beam Accelerometer technology and Quartz Pendulous Accelerometer technology. Since their roll out in the '90s, Quartz Pendulous Accelerometers rapidly became the most widely used accelerometers for high grade navigation applications and this position remains largely unchallenged to this time.

InnaLabs® Ltd. is a privately held limited company which was incorporated in Ireland in 2011. The Company has recently completed the development of a range of specialist precision Quartz Pendulous Accelerometers which are today used in a variety of navigation and tactical applications.

After a brief description of the basic physical principles and an overview of the key manufacturing processes developed by Innalabs, such as the quartz wet etching, this paper provides statistical results recorded on the AI-Q-2010, AI-Q-1410 and AI-Q-710 accelerometer variants. These three part numbers are currently in full series production in Dublin. Some key performance parameters are presented, such as the bias and scale factor stability over temperature and over time, the short-term bias stability (measured using the Allan variance method), the output noise, and the sensitivity to shock and vibration.

The results presented here demonstrate the capabilities of the InnaLabs® Quartz Pendulous Accelerometer range. These products provide a European source of high grade accelerometers for applications requiring navigation and tactical grade performance.

1. Introduction

The principles of Quartz Pendulous Servo Accelerometers are well known with the first highly efficient designs being disclosed in the late '60s by Wilcox [1] [2] (North American Aviation, 1966 – 1967), Rogall [3] (Singer General Precision, 1970) and E. Jacobs [4] (Sundstrand Data Control, 1972). At that time two types of design predominated, both covering the needs for high accuracy navigation systems down to guidance systems: the Pendulous Integrated Gyro Accelerometer (PIGA) and the Floated Pendulum Accelerometer. As new systems being developed were not targeting extremely high

accuracy but instead smaller size, higher reliability and better cost, the industry research effort was therefore focused on new innovative concepts with a significantly reduced number of mechanical parts (see Figure 1.). Dry Pendulous Servo Accelerometers and Vibrating Beam Accelerometers (VBA) were then conceived and took over on the navigation and tactical grade market segment from the late ‘70s to the ‘90s. Gradually Floated Pendulum Accelerometers were replaced and PIGAs were confined to ballistic missile applications. MEMS accelerometer technology is also part of this trend with the first micro machined accelerometer fabricated at Stanford University in 1979 [5]. Although the initial stage was mainly focused on high volume commercial applications (e.g. Automotive) and manufacturing technologies (e.g. DRIE), the activity on MEMS inertial sensors really picked-up in the ‘2000s:

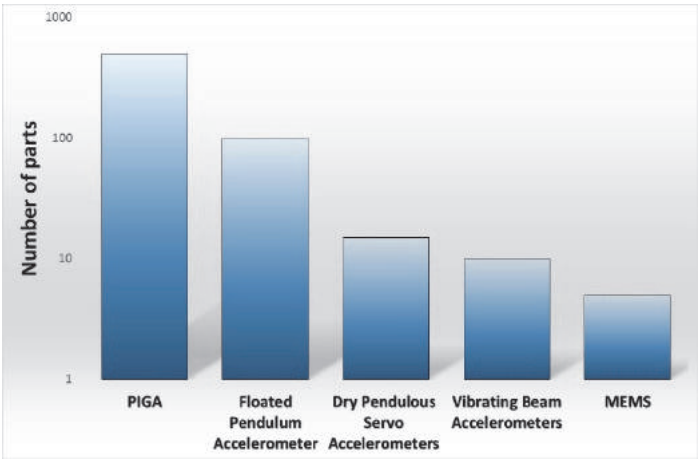

Figure 1. Technology variants versus mechanical complexity

In Figure 1. MEMS is identified as a separate group but in reality this group overlaps Dry Pendulous Servo Accelerometers and VBAs. As VBAs appeared to be sensitive to mechanical environments and MEMS were seemingly a good fit to low grade tactical applications (e.g. >100µg to few mg), Dry Pendulous Servo Accelerometers rapidly became the most widely used accelerometers for navigation and high grade tactical applications. In particular, the Quartz variant initially developed by Sundstrand Data Control in the late ‘90s [6] is today seen as the de-facto industry standard in the open market.

Following in the footsteps of these pioneers and after the launch of its tactical grade Coriolis Vibratory Gyroscopes [7] [8], InnaLabs® recently introduced the AI-Q-2010, AI-Q-1410 and AI-Q-710 Quartz Pendulous Servo Accelerometers. These Accelerometers are the latest addition to InnaLabs® quality line of high performance “built in Europe” and ITAR-Free sensors targeted at navigation, tactical, control and measurement applications.

2. Technology and Design Principles

The core of the proof mass or seismic mass of InnaLabs® pendulous accelerometers is a high purity fused quartz disc structure (the flapper) connected to a rigid outer frame by two thin hinges. The overall structure is monolithic and a deposited Au film is used to form an electrode pattern onto the surface of the pendulum as required for capacitive detection and for connection to the torque conducting leads (see Figure 2.a.).

Fabrication of InnaLabs® pendulum is based on conventional wet etching techniques and is categorised as a wafer based process. As the fused quartz material used consists of quartz in amorphous form, the etching is isotropic and produces a high quality surface finish without surface defects as typically observed for crystalline materials. The etching is performed simultaneously from both sides of the pendulum in the deep cavity locations and thus the overall symmetry is well preserved and leads to dimensional accuracy circa 1µm. Therefore, with an etch rate of ~3µm/min, pendulums are volume produced at high yield.

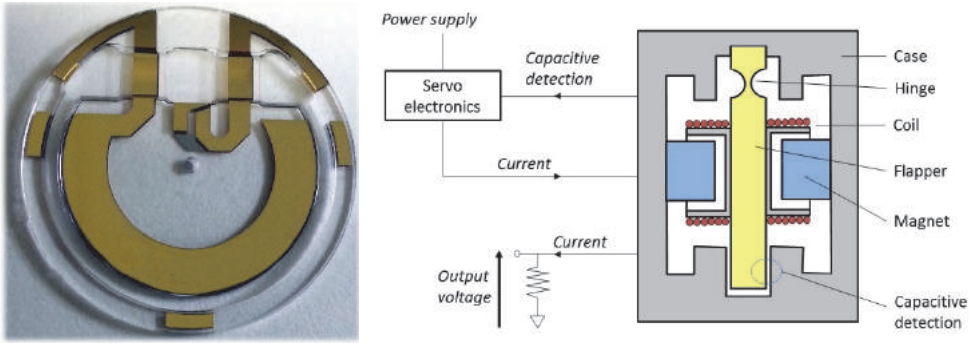

Figure 2.a. Fused Quartz Pendulum – 2.b. Outline schematic

The outer frame is clamped symmetrically between two magnetic structures comprising a high stability magnet and a nickel–iron alloy case, the overall structure forming an accelerometer cell. A small gap of ~20µm is left between the flapper and the magnetic structure in order to obtain a system of two capacitor plates on each side of the flapper for capacitive detection and for squeeze film damping. When acceleration is applied perpendicularly to the proof mass, a servo loop circuit derives an error signal from the capacitive detection and delivers a current into two coils attached symmetrically to each side of the flapper. Laplace forces are then applied to the winding and therefore the proof mass will be maintained in a capture or null mode with its centre in a null position, over a broad frequency band of input accelerations (i.e. >2 kHz typical). As the current through the coils is proportional to the applied acceleration, the same current flowing through an external load resistor will then generate an output voltage proportional to acceleration (see Figure 2.b.).

The cell is connected to an electronics proximity board which contains the servo loop for controlling the pendulum angular position and a thermal sensor. These parts are attached into a hermetically sealed metal housing to form a complete accelerometer of which Figure 3. shows examples for the AI-Q-2010, AI-Q-1410 and AI-Q-710 variants. The internal sensor cell components used in the accelerometers are identical for the AI-Q-710 and AI-Q-1410, the only difference being the outer housing, which provides an alternative mounting arrangement. The AI-Q-2010 contains higher-grade internal sensor cell components providing enhanced performance. Identical electronic control boards are used in all three variants.

Figure 3. – AI-Q-2010, AI-Q-1410 and AI-Q-710 variants

3. Design Rationale

A set of vectors $\boldsymbol{IA}$, $\boldsymbol{PA}$ and $\boldsymbol{OA}$ as shown in Figure 4.a. is typically used to define the three principal axes of a pendulous accelerometer [9]. Figure 4.b. presents a conceptual drawing for the pendulous accelerometer for which five forces $\boldsymbol{F}$, $\boldsymbol{R}$, $\boldsymbol{f_e}$, $\boldsymbol{f_d}$ and $\boldsymbol{T}$ are shown, all parallel to $\boldsymbol{IA}$ for the sake of simplicity. These forces respectively refer to the inertial force applied to the accelerometer, the reaction force at the pivot point, a restoring elastic force primarily generated by the hinges when the proof mass is displaced, the squeeze film damping force and the Laplace force applied to the pendulum.

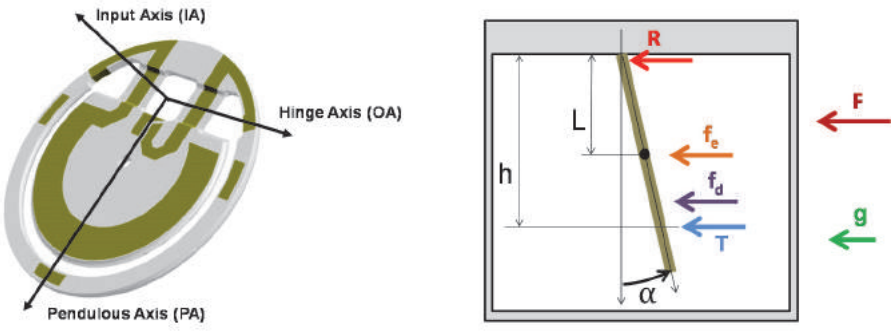

Figure 4.a. Axes of a pendulous accelerometer – 4.b. Conceptual drawing

These forces are applied to different points with different lever-arms. h denotes the lever-arm for $\boldsymbol{T}$. L is the position of the centre of mass. The gravitational field is denoted $\boldsymbol{g}$ and purposely oriented parallel to $\boldsymbol{IA}$. The angle deflection of the pendulum is denoted α. The dynamic response of this system can then be simply derived from Newton's laws of motion applied to the overall accelerometer and to the pendulum. As a result, angle α is the solution to the following second order differential equation using two time constants τ_1 and τ_2:

$$\tau_1\tau_2\ddot{\alpha} + \tau_2\dot{\alpha} + \alpha = \frac{1}{L.{\omega_0}^2}(a_i - a_{ACC})\ ,\ \tau_1 = \frac{J}{C}\ ,\ \tau_2 = \frac{C}{k}\ ,\ {\omega_0}^2 = \frac{k}{L.P} \qquad (1)$$

In Equation (1), J is the moment of inertia about the hinge axis $\boldsymbol{OA}$, C is the damping torque coefficient, k is the rotational stiffness due to the restoring elastic torques, P is the pendulosity (i.e. $P = mL$~0.55g.cm, with m the mass of the pendulum), ω_0 is an angular frequency, and a_i and a_{ACC} the applied specific force along $\boldsymbol{IA}$ and the accelerometer acceleration output respectively. Based on the above model, a_i and a_{ACC} take the following form, with M the mass of the accelerometer:

$$a_i = \frac{F}{M}\ \ ,\ a_{ACC} = \frac{Th}{P} \qquad (2)$$

As a case study, let's consider first a non-feedback configuration for which the angle deflection becomes the signal driving the accelerometer output. Given the symmetry of the system and materials used, the rotational stiffness k is typically a small number (~5 10^{-4} N.m/rad) and $\tau_1 \ll \tau_2$.

Therefore the following approximation can be made, $\tau_2 \approx \tau_1 + \tau_2$, and the Laplace transform of Equation (1) takes the following form, with s the Laplace operator:

$$\frac{\alpha(s)}{a_i(s)} = K_{OL}(s) = \frac{\frac{1}{L.{\omega_0}^2}}{1+\tau_2 s+\tau_1\tau_2 s^2} \approx \frac{\frac{1}{L.{\omega_0}^2}}{(1+\tau_1 s)(1+\tau_2 s)} \qquad (3)$$

Equation (3) shows the open-loop system behaves as a second order low pass filter with a slope -1 up to $f_1 = \frac{1}{2\pi\tau_1}$ and a slope -2 above f_1 due to squeeze film damping.

Not surprisingly, the resonant frequency f_{OL} is defined by the mechanical properties of the hinges and the moment of inertia of the pendulum about its hinge axis:

$$f_{OL} = \frac{1}{2\pi\sqrt{\tau_1\tau_2}} = \frac{1}{2\pi}\sqrt{\frac{k}{J}} \tag{4}$$

With L = 8 mm, the resonant frequency is 17 Hz. This highlights clearly a trade-off between sensitivity and accuracy as the rotational stiffness should be increased in order to achieve a larger bandwidth, but unfortunately, this comes through sacrificing the bias performance. In addition, cross-coupling errors, pickoff nonlinearities and mechanical hysteresis of the hinges (as the proof mass is displaced) raise some other technical challenges worth considering for that specific configuration. Ultimately, and despite its apparent simplicity, the open-loop configuration exhibits inherent limitations leading to the choice of a closed-loop configuration for high accuracy systems.

In order to strengthen this idea, let's consider the following Figure 5. showing the block diagram applicable to InnaLabs® closed-loop pendulous accelerometers:

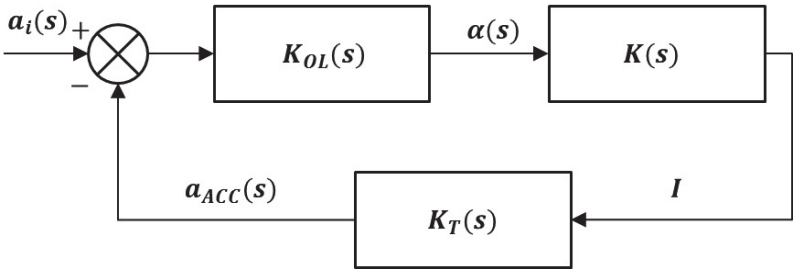

Figure 5. Block diagram

In Figure 5., $K(s)$ is a transfer function which includes an amplitude modulation of the capacitive detection signals (proportional to angle α), a synchronous demodulation, a PID controller and a current amplifier generating a current I previously shown in Figure 2.b. $K_T(s)$ is the transfer function reflecting the physical process for which the current I becomes a restoring torque applied to the pendulum. Let's denote H as the product $K.K_T$. As a result of the above, the overall transfer function for the accelerometer takes the following form, with $K_{OL}(s)$ given by Equation (3):

$$\frac{a_{ACC}}{a_i} = \frac{K_{OL}\times H}{1+K_{OL}\times H} \tag{5}$$

To make it simple, let's assume H is a constant. By design H is large ($\gg$100ms^{-2}) and then Equation (5) takes the following simplified form:

$$\frac{a_{ACC}}{a_i} \approx \frac{1}{1+\frac{L.\omega_0{}^2}{H}\tau_2 s+\frac{L.\omega_0{}^2}{H}\tau_1\tau_2 s^2} \tag{6}$$

Equation (6) shows the static gain is 1 and consequently, for low frequencies, the accelerometer output a_{ACC} is a direct measure of the specific force a_i applied to the accelerometer along $\boldsymbol{IA}$:

$$a_{ACC} = a_i \tag{7}$$

The resonant frequency is given by the following equation:

$$f_{CL} = \frac{1}{2\pi}\sqrt{\frac{HP}{J}} \approx \frac{1}{2\pi}\sqrt{\frac{H}{L}} \tag{8}$$

Therefore, as expected, the bandwidth of the system does not depend any more on the rotational stiffness and, by using an appropriate electronics gain H, the bandwidth can be extended to high values, typically beyond 1 kHz.

By considering Equation (2), and given the fact that the force T is a Laplace force generated by windings of length l carrying a current I in a magnetic field B, Equation (7) becomes:

$$\frac{I}{K_1} = a_i \ , K_1 = \frac{P}{Blh} \tag{9}$$

As the current I is the real accelerometer output signal, parameter K_1 as defined by (9) is finally the scale factor of the closed-loop accelerometer, with mA/g as typical units.

Equation (9) is the model equation of an ideal pendulous servo accelerometer under static conditions (i.e. shock and random vibrations excluded). Depending on application requirements, this model equation is generally complemented by several error parameters reflecting to varying degrees the operational behaviour of the accelerometer and the effect of manufacturing and material defects [9]. In the following, the model equation considered will be limited to the most common error parameters and (9) becomes:

$$\frac{I}{K_1} = K_0 + a_i + K_2 a_i{}^2 + \delta_o a_p - \delta_p a_o \tag{10}$$

Parameters K_0, K_2, δ_o and δ_p are respectively the bias (g), the second order coefficient (g/g^2), the misalignment angle between $\boldsymbol{IA}$ and $\boldsymbol{PA}$, and the misalignment angle between $\boldsymbol{IA}$ and $\boldsymbol{OA}$. a_p and a_o are applied acceleration components along $\boldsymbol{PA}$ and $\boldsymbol{IA}$.

4. Results and Performance Achieved

The key parameters defined above are measured in accordance with IEEE Std 1293-1998 [9]. Qualification results for the navigation grade (AI-Q-2010), tactical grade (AI-Q-1410) and measurement grade (AI-Q-710) accelerometers are presented below. During testing, all data is recorded to a database system, to allow for full statistical analysis and statistical process control.

The charts in Figure 6 show the measured transfer functions of the InnaLabs® accelerometers, and are consistent with the equations developed in section 3. The measurements were taken using the electronic bandwidth method, in which an electronic stimulus is injected into the control loop and the subsequent response measured. This technique has been compared to the mechanical bandwidth response and yields consistent results.

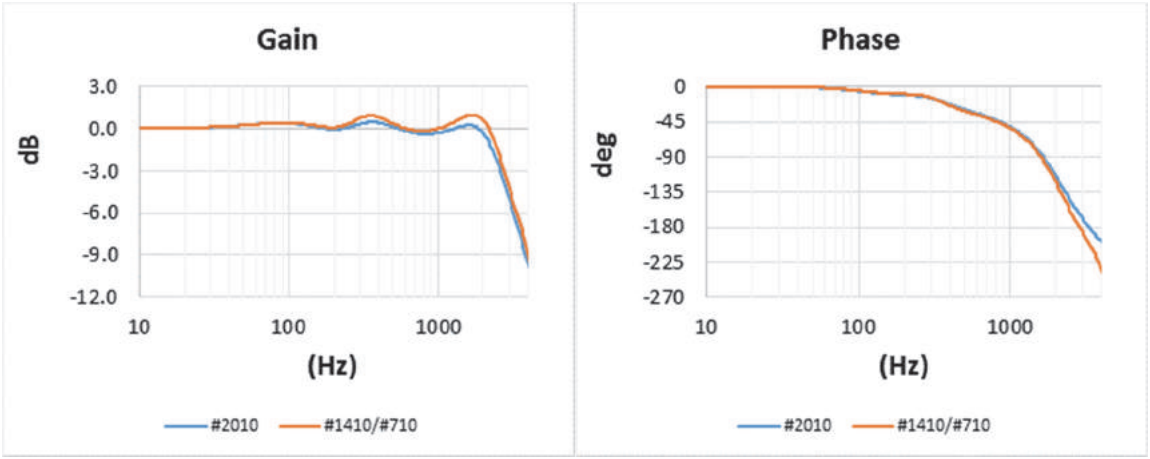

Figure 6. Transfer functions

In the Table 1 below, the bandwidth parameters have been extracted from the data shown above. The system model described in section 3 (equation 6) is based upon a second order system. This is a good approximation for the observed gain responses, however the phase responses are more accurately modelled using a third order fit. As expected, the results are consistent across all variants due to the use of common control electronics.

Type	Bandwidth at 90°	Bandwidth at -3dB	Damping factor	Specification
AI-Q-2010	1660 Hz	2600 Hz	ζ =0.55	$\geq 300Hz\ (-3dB)$
AI-Q-1410 & 710				$\geq 300Hz\ (90°)$

Table 1. Bandwidth characteristics

The following charts show the distributions of the bias, scale factor and misalignment, recorded during the temperature testing. After the charts for each parameter, the statistical data is presented in tabular form. Testing of the accelerometer is performed using an indexing table with resolution and an accuracy of <1 μrad. The accelerometers are mounted on a precision machined fixture inside by a thermal chamber. The ramp rate between 2 consecutive set points is 3°C/min and the temperature stability required on each set-point is ±0.2°C.

The bias, K_0, is calculated from a four-position test over temperature as per reference [9]. This is done by summing the ±1g measurements from the test, which gives the offset from zero of the accelerometer output. The thermal sensitivity of the bias is calculated as the slope of a first order least squares fit to the bias results over the full operating temperature range of -55°C to +95°C. The bias at room temperature and thermal slope distribution functions are shown in Figure 7.

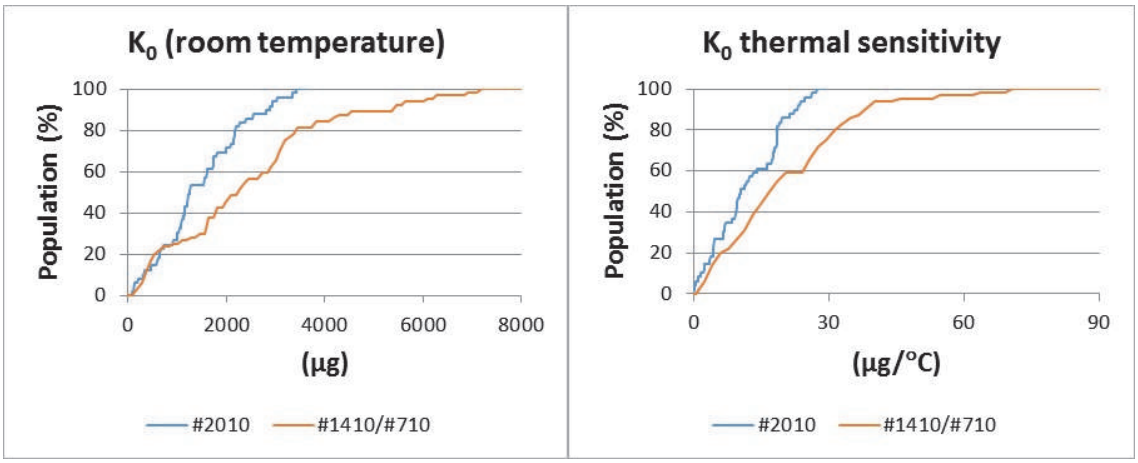

Figure 7. K_0 at room temperature and K_0 thermal sensitivity (uncompensated)

The bias residuals are calculated by subtracting a third order least squares model from the raw data over the full operating temperature range. From this, the largest absolute value is taken as the bias hysteresis. An example of the bias residuals and the hysteresis distribution function are shown in Figure 8.

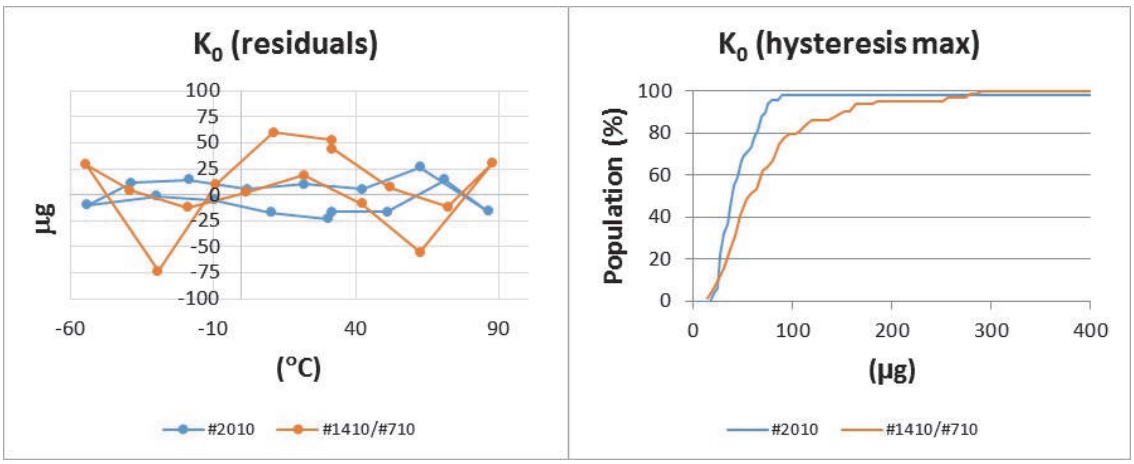

Figure 8. K_0 residuals over temperature – Example (Left), Statistics (Right)

The bias data in Table 2 below was extracted from the distribution functions shown in Figures 7 and 8 above. The InnaLabs® specification limits are shown for reference. The 50% and 70% data represents the bias limit values within which 50% and 70% of the accelerometer population falls.

Parameter	Units	50%	70%	Type	Specification
K_0 at room temperature	μg	≤1,250	≤1,950	AI-Q-2010	<4,000
		≤2,200	≤3,100	AI-Q-1410	<5,000
				AI-Q-710	<8,000
K_0 thermal sensitivity	$\mu g/℃$	≤10	≤20	AI-Q-2010	<30
		≤20	≤30	AI-Q-1410	<70
				AI-Q-710	<70
K_0 residuals over temperature (hysteresis)	μg	≤40	≤50	AI-Q-2010	*Proprietary information*
		≤60	≤90	AI-Q-1410	
				AI-Q-710	

Table 2. Bias performance and specification limits

The bias values for the AI-Q-1410 and AI-Q-710 populations are grouped together due to the design similarities and are somewhat higher than the corresponding AI-Q-2010 values.

The AI-Q-2010 K_0 data shows that ~70% of the parts have a bias offset of below half of the specification limit. For the thermal bias sensitivity the 70% level is at two thirds of the specification. For all variants, the bias hysteresis is also comfortably within the InnaLabs® proprietary specification limits indicating that, for this parameter, many of the parts are performing to a higher accelerometer classification level.

The scale factor, K_1, data distribution functions are given below. Scale factor is also calculated from the four-position test over temperature as per reference [9]. The thermal parameters of the scale factor (slope and hysteresis) are calculated in the same way as the bias parameters. The distribution functions for scale factor at room temperature and thermal slope are shown in Figure 9.

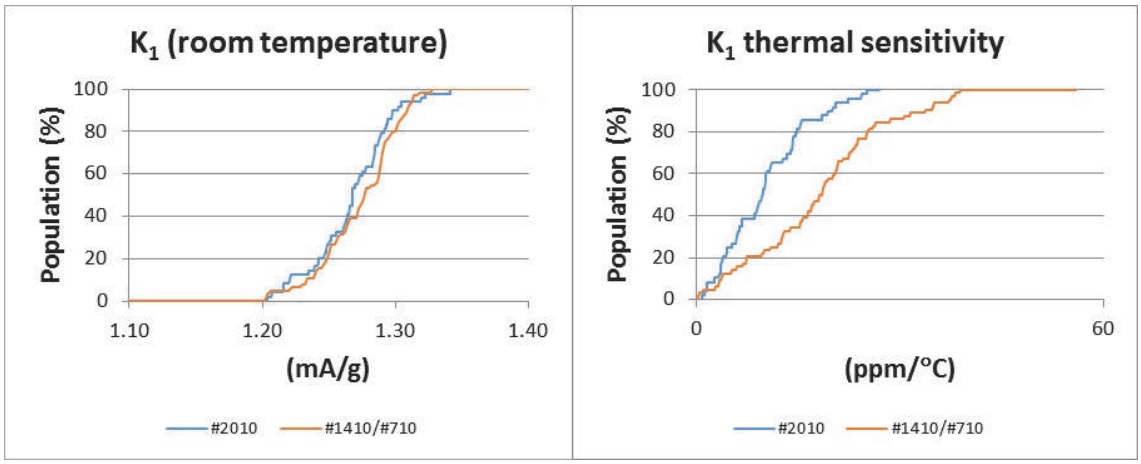

Figure 9. K_1 at 30 °C and K_1 thermal sensitivity (uncompensated)

An example of the scale factor residuals and the hysteresis distribution function are shown in Figure 10.

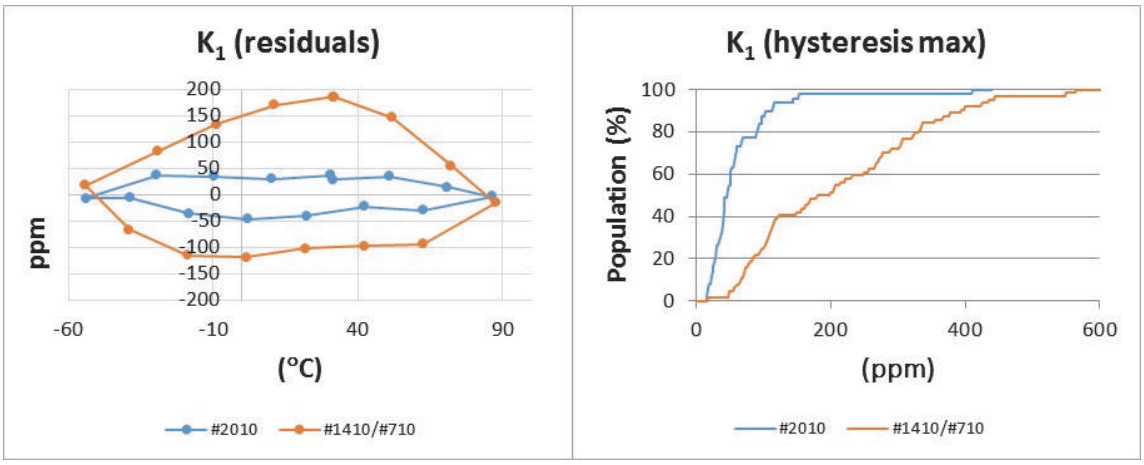

Figure 10. K_1 residuals over temperature – Example (Left), Statistics (Right)

The scale factor data in Table 3 below was extracted from the distribution functions shown in Figures 9 and 10, above. The InnaLabs® specification limits are shown for comparison.

Parameter	Units	50%	70%	Type	Specification
K_1 at room temperature	mA/g	1.27 (mean)	1.26 to 1.28	AI-Q-2010	1.20 to 1.46
		1.28 (mean)	1.26 to 1.29	AI-Q-1410	1.20 to 1.46
				AI-Q-710	1.23 to 1.43
K_1 thermal sensitivity	ppm/°C	≤10	≤15	AI-Q-2010	<180
		≤20	≤25	AI-Q-1410	<180
				AI-Q-710	<200
K_1 residuals over temperature (hysteresis)	ppm	≤45	≤60	AI-Q-2010	*Proprietary information*
		≤200	≤300	AI-Q-1410	
				AI-Q-710	

Table 3. Scale factor performance and specification limits

For all variants, the scale factor thermal sensitivity is significantly below the specification limit indicating that, for this parameter, many of the parts are performing to a higher accelerometer classification level. The scale factor hysteresis is also comfortably within InnaLabs® proprietary specification limits for the majority of these parts. As with the bias parameters, the AI-Q-1410 and AI-Q-710 populations exhibit a wider performance distribution within the specification limits due to the sensor cell design employed.

The misalignment data distribution functions are given below. Misalignment is calculated from the four-position test over temperature as per reference [9], using the output value at two different 0g. This is converted to a misalignment value based on the small angle approximation.

The thermal parameters of the misalignment (slope and hysteresis) are calculated in the same way as the bias and scale factor parameters. The distribution functions for misalignment at room temperature and thermal slope are shown in Figure 11. Only the output axis misalignment (δ_o) is shown, as the pendulous axis misalignment (δ_p) gives consistent results.

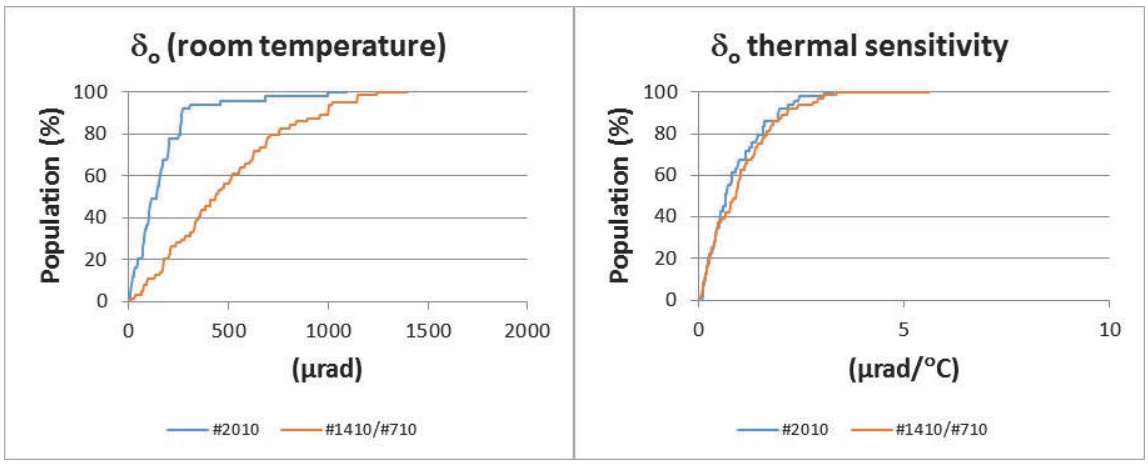

Figure 11. δ_o at room temperature and δ_o thermal sensitivity (uncompensated)

An example of the misalignment residuals and the hysteresis distribution function are shown in Figure 12.

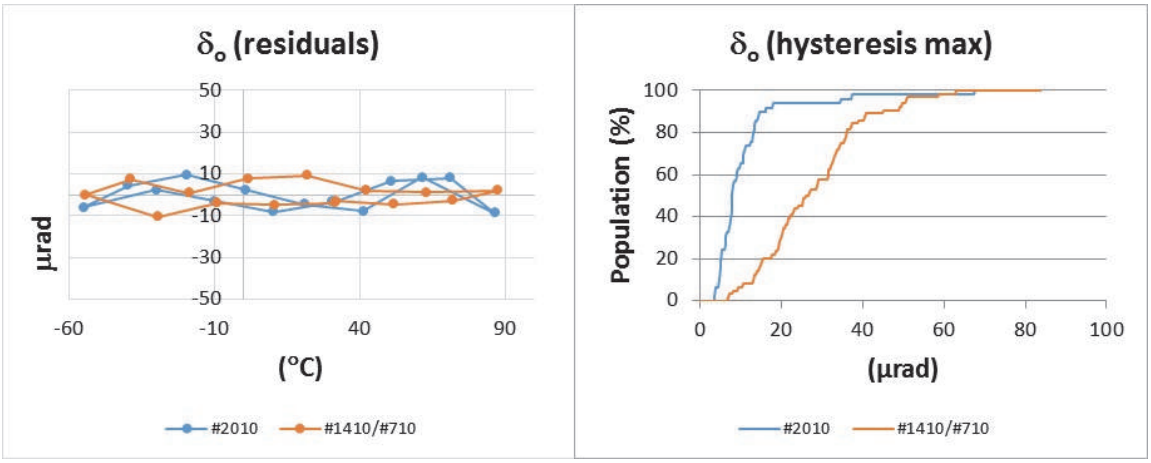

Figure 12. δ_o residuals over temperature – Example (Left), Statistics (Right)

The misalignment data in Table 4 below was extracted from the distribution functions shown in Figures 11 and 12, above. For all variants, the room temperature misalignment, thermal sensitivity and stability are all comfortably within the specification limits and exhibit performance consistent with a higher classification quartz pendulous accelerometer.

Again the corresponding data for the AI-Q-1410 and AI-Q-710 populations exhibit a wider performance distribution within the specification limits.

Parameter	Units	50%	70%	Type	Specification
δ_o at room temperature	µrad	≤140	≤200	AI-Q-2010	<2,000
		≤440	≤660	AI-Q-1410	
				AI-Q-710	
δ_o thermal sensitivity	µrad/℃	≤1.5	≤2	AI-Q-2010	*Proprietary information*
		≤1.5	≤2	AI-Q-1410	
				AI-Q-710	
δ_o residuals over temperature (hysteresis)	µrad	≤10	≤15	AI-Q-2010	
		≤30	≤50	AI-Q-1410	
				AI-Q-710	

Table 4. Misalignment data and specification limits

In order to assess the noise content and short term stability of the accelerometer, two tests were performed as part of the qualification programme: Spectral noise and Allan Variance.

The Allan Variance test was performed by recording a one hour of data from the accelerometer and calculating the standard deviation of different time averages of the data. The Allan Variance is shown in Figure 13.

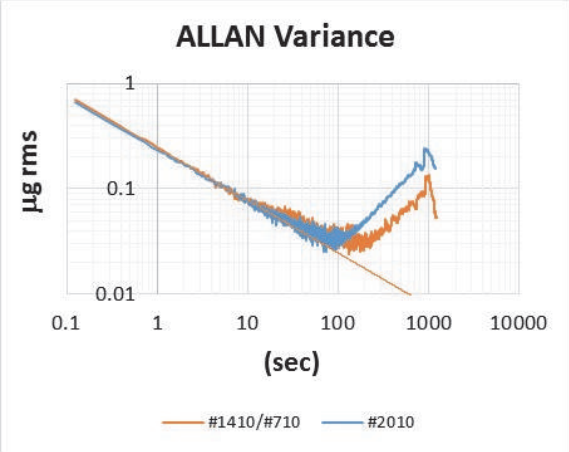

Figure 13. Allan Variance

The characteristics of the Allan Variance are dominated by the control electronics and are therefore very similar for all accelerometer variants which use the same control boards. For all variants, the lowest point achieves an outstanding 30 nano g rms value at 100 seconds along with a Velocity Random Walk circa 15 µg.s/√hr consistent with a higher classification quartz pendulous accelerometer.

The Allan Variance figures taken from the InnaLabs accelerometer qualification testing are shown in Table 5 below.

Parameter	Units	Typical	Type	Specification
Bias instability (Lowest point of Allan Variance)	µg rms	0.03	AI-Q-2010	*Proprietary information*
			AI-Q-1410	
			AI-Q-710	
Velocity Random Walk	µg.s/√hr	14	AI-Q-2010	
			AI-Q-1410	
			AI-Q-710	

Table 5. Allan deviation parameters

The spectral noise test was performed using a spectrum analyser and measures the noise content of the frequency ranges of interest (0.1 Hz to 10 kHz for the InnaLabs® accelerometers). The spectral noise figures taken from the InnaLabs® accelerometer qualification testing are shown in Table 6 below, compared to the InnaLabs® specification.

Parameter	Units	Typical	Type	Specification
0 – 10Hz	µg rms	0.02	AI-Q-2010	<7
		0.5	AI-Q-1410	
			AI-Q-710	
10 – 500Hz		20	AI-Q-2010	<70
		45	AI-Q-1410	
			AI-Q-710	
500 – 10,000Hz		500	AI-Q-2010	<1500
		500	AI-Q-1410	
			AI-Q-710	

Table 6. Spectral noise performance

The spectral noise for all variants is comfortably below the specification limits across the entire spectral range.

As per reference [9], the long term repeatability figures are derived from a test for which the measurements are taken under constant conditions and between successive measurements, the accelerometers are exposed to temperature variations. For this purpose, a real-time ageing programme was initiated, in which a four-position test over temperature is performed every 2 weeks. In between tests, the accelerometers are stored in normal storage conditions (ambient temperature and atmosphere). The charts in Figure 14 show the results to date. 100 days of data has been gathered from 3 randomly chosen units and testing is ongoing. The worst-case (i.e. max. value) results were taken from the recorded data.

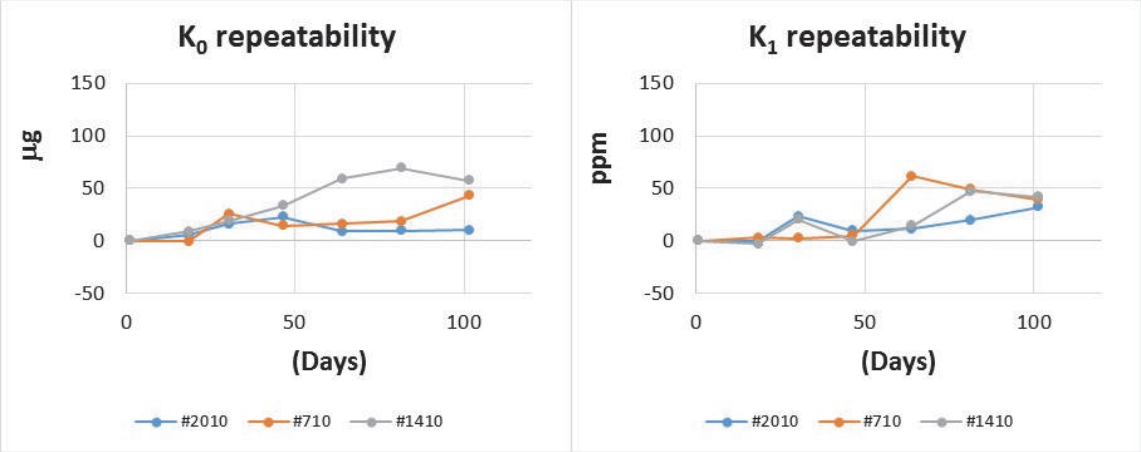

Figure 14. K0 and K1 repeatability (worst case across 3 temperatures)

The 3σ values are given in Tables 7 and 8 below for the bias and scale factor.

Parameter	Units	Measured	Type	Specification
K_0 repeatability	µg	20 (100 days)	AI-Q-2010	<550 (1 year)
		70 (100 days)	AI-Q-1410	<1000 (1 year)
			AI-Q-710	<1200 (1 year)

Table 7. Bias repeatability

Parameter	Units	Measured	Type	Specification
K_1 repeatability	ppm	50 (100 days)	AI-Q-2010	<600 (1 year)
		80 (100 days)	AI-Q-1410	<1000 (1 year)
			AI-Q-710	<1200 (1 year)

Table 8. Scale factor repeatability

While the measurements have yet to complete the full 1 year target time, the data thus far suggests that the final values should be significantly within the specification limits for all accelerometer variants. Testing will continue up to and beyond the 1 year value and additional units will be added to the test as appropriate to increase the volume of data available.

During the qualification test programme, all three variants of InnaLabs accelerometer were subjected to vibration and shock testing in all three axes. Vibration testing consisted of sine sweep and random vibration in the frequency range 20 Hz – 2 kHz. The sine sweep profile applied accelerations of up to 35 g, while random vibration was applied at 14 g_{RMS}. Shocks were applied at 70 g (11 ms), 110 g (8 ms) and 250 g (4 ms). Following the testing, the results were compared to those taken before the shock and vibration testing. The changes observed to the performance of the accelerometer were negligible when compared to the performance before testing.

Part of the measurements is the vibration rectification error (VRE) test, in which a bias offset caused by in-plane vibration is measured. The VRE distributions are shown below for a sample of each accelerometer variant. The test limits for each frequency range are marked as dashed lines.

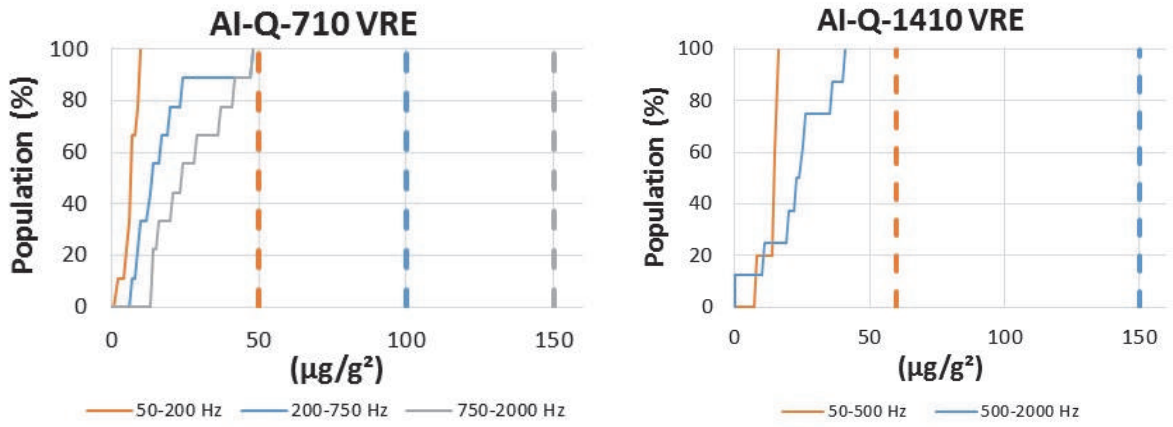

Figure 15. AI-Q-710 and AI-Q-1410 VRE Results Distribution

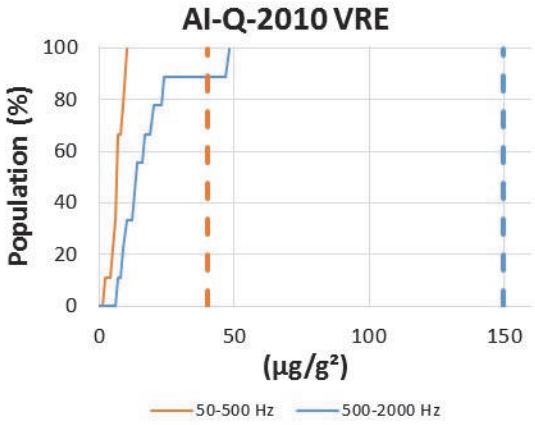

Figure 16. AI-Q-2010 VRE Results Distribution

For all variants the measure values of VRE are significantly below the specification limits for each of the frequency ranges.

The data in Table 9 is extracted from the VRE data shown in the charts above.

Parameter	Units	50%	70%	Frequency Range	Specification
AI-Q-710 VRE	µg/g²	6	7	50-200 Hz	<50
		14	20	200-750 Hz	<100
		24	40	750-2000 Hz	<150
AI-Q-1410 VRE		15	16	50-500 Hz	<60
		23	26	500-2000 Hz	<150
AI-Q-2010 VRE		7	10	50-500 Hz	<40
		25	32	500-2000 Hz	<150

Table 9. VRE Distribution Parameters

8. Conclusion

The design, construction and operating principles of InnaLabs® recently released range of quartz pendulous accelerometers have been described. Three accelerometer variants have been produced: the navigation grade AI-Q-2010, the AI-Q-1410 tactical grade and the AI-Q-710 which delivers industrial grade performance. The results of an extensive test and qualification campaign are presented highlighting the key performance characteristics of these accelerometers.

This accelerometer range is manufactured and tested at InnaLabs® facility in Dublin, Ireland and therefore provides a European source of high quality parts for a wide range of markets and applications. The performance of these accelerometers are fully compliant with widely recognised industry standard specifications for quartz pendulous accelerometer technology.

When comparing the demonstrated performance of the AI-Q2010 to these specifications, it is clear that this design has the potential to deliver performance consistent with higher grades of accelerometer. Work is ongoing at Innalabs to further develop this technology to enable these higher grade accelerometers to be added to the AI-Q-XXXX product portfolio in the near future.

References

[1] D. Wilcox, “Accelerometer”, U.S. Patent 3,229,530

[2] D. Wilcox, “Accelerometer”, U.S. Patent 3,333,419

[3] H. Rogall, “Sub-miniature Single Axis Accelerometer”, U.S. Patent 3,513,711

[4] E. Jacobs, “Accelerometer”, U.S. Patent 3,702,073

[5] L.M. Roylance, J.B. Angell, “A Batch-Fabricated Silicon Accelerometer”, IEEE Transactions on Electron Devices, vol. ed-26, no. 12, December 1979

[6] S.A. Foote, D.B. Grindeland, “Model QA3000 Q-Flex® Accelerometer. High Performance Test Results”, IEEE AES Magazine, June 1992

[7] J. Beitia, C. Fell et al., “High-grade CVG for Stabilisation Control Systems and Tactical Grade Systems”, Proceedings of the Gyro Technology Symposium, Germany 2013

[8] J. Beitia, C. Fell et al., “Low Cost CVG for High-grade North Finders and Targeting Systems”, Proceedings of the Gyro Technology Symposium, Germany 2014

[9] IEEE Std 1293-1998, “Guide and Test Procedure for Linear, Single-Axis, Non-gyroscopic Accelerometers”, Proceedings of the Gyro Technology Symposium, Germany 2014